Modeling the Dissociation Conditions of Salt Hydrates and Gas Semiclathrate Hydrates: Application to Lithium Bromide, Hydrogen Iodide, and Tetra- n -butylammonium Bromide + Carbon...

ARTICLE *in* THE JOURNAL OF PHYSICAL CHEMISTRY B · JANUARY 2011

Impact Factor: 3.3 · DOI: 10.1021/jp1067457 · Source: PubMed

1 AUTHOR:

Patrice Paricaud
ENSTA-ParisTech, Université Paris-Saclay
42 PUBLICATIONS **819** CITATIONS

SEE PROFILE

Modeling the Dissociation Conditions of Salt Hydrates and Gas Semiclathrate Hydrates: Application to Lithium Bromide, Hydrogen Iodide, and Tetra-*n*-butylammonium Bromide + Carbon Dioxide Systems

Patrice Paricaud*

UER Chimie et Procédés, ENSTA-ParisTech, 32 Boulevard Victor, 75739 Paris Cedex 15, France

Received: July 20, 2010; Revised Manuscript Received: October 23, 2010

A thermodynamic approach is proposed to determine the dissociation conditions of salt hydrates and semiclathrate hydrates. The thermodynamic properties of the liquid phase are described with the SAFT-VRE equation of state, and the solid−liquid equilibria are solved by applying the Gibbs energy minimization criterion under stoichiometric constraints. The methodology is applied to water + halide salt systems, and an excellent description of the solid−liquid coexistence curves is obtained. The approach is extended to the water + tetra-*n*-butylammonium bromide (TBAB) binary mixture, and an accurate representation of the solid−liquid coexistence curves and dissociation enthalpies is obtained. The van der Waals−Platteeuw (vdW−P) theory combined with the new model for salt hydrates is used to determine the dissociation temperatures of semiclathrate hydrates of TBAB + carbon dioxide. A good description of the dissociation pressures of CO_2 semiclathrate hydrates is obtained over wide temperature, pressure, and TBAB composition ranges (AAD = 10.5%). For high TBAB weight fractions the new model predicts a change of hydrate structure from type A to type B as the partial pressure of CO_2 is increased. The model can also capture a change of behavior with respect to TBAB concentration, which has been observed experimentally: an increase of the TBAB weight fraction leads to a stabilization of the gas semiclathrate hydrate at low initial TBAB concentrations below the stoichiometric composition but leads to a destabilization of the hydrate at TBAB concentrations above the stoichiometric composition.

1. Introduction

Salt hydrates, also called hydrated ionic compounds, are solid compounds (or solid complexes) formed by combination of the ions with a definite number of water molecules. Electrolyte aqueous systems such as lithium halide systems[1] can exhibit several hydrates over the liquid composition range, which differ in structure and hydration number. Salt hydrates can be used as phase change materials (PCM) to store thermal energy. Electrolyte solutions such as lithium halide or calcium chloride solutions have been used in absorption refrigeration machines and absorption heat pumps. For these systems it is important to know the solid−liquid equilibrium boundaries, as crystallization can cause serious problems during operation. The modeling studies for these systems are rather scarce. Solid−liquid equilibria involving salt hydrates have been modeled by using the modified Brunauer, Emmett, and Teller (BET) theory.[2−4] The BET approach is particularly useful for modeling solid−liquid equilibria (SLE) at high salt concentration. One can also mention the work of Wang et al.,[5] who applied an electrolyte thermodynamic model based on the Pitzer−Debye−Hückel model to calculate the solubilities of $CaCl_2$ hydrates. However, electrolyte equations of state have never been applied to determine the dissociation conditions of salt hydrates.

Another class of salt hydrates is semiclathrate hydrates of tetraalkylammonium salts. These hydrates exhibit a water−anion framework with empty dodecahedral cavities and large cavities that contain the alkyl chains of the cations.[6] Fowler et al.[7] were among the firsts to form semiclathrate hydrates of tetraalkylammonium salts. Tetraalkylammonium halide aqueous solutions have been extensively studied as they have many industrial applications: for instance, tetra-*n*-butylammonium bromide (TBAB) is used as an intermediate reactant and as a phase transfer catalyst. Moreover, tetraalkylammonium halide solutions have been studied as model solutions to try to understand the nature of hydrophobic interactions and the structuring of water molecules around large apolar solutes. The phase behavior of tetra-*n*-butylammonium bromide (TBAB) + water system is rich and complex, as it exhibits vapor−liquid equilibria[8] at low pressures, liquid−liquid equilibria at very high pressures,[9] ion pairing at moderate concentrations,[10] and a complex solid−liquid phase diagram.[11,12] Some physical properties of tetraalkymammonium cations in aqueous solution have been recently reviewed by Marcus.[13] The solid−liquid phase diagrams of tetraalkylammonium halide salts + water binary systems have been reviewed by Dyadin and Udachin[11] and Aladko et al.[14] The solid−liquid phase diagram of the TBAB + H_2O system exhibits different hydrates for TBAB weight fractions inferior to 60%. The structures and stoichiometric compositions of these hydrates have been the object of controversy: according to Nakayama[15] a hydrate of hydration number $\nu_w = 24$ is formed; Dyadin and Udachin[11] found four different hydrates of hydration numbers $\nu_w = 24$, 26, 32, and 36; Shimada and co-workers[12,16−18] found only two kinds of hydrates denoted as types A and B of hydration numbers $\nu_w = 26$ and 38, respectively. The solid−liquid phase behavior of tetraalkymammonium salt + water binary systems is complex, and no thermodynamic model has ever been developed to determine the SLE in these systems to our knowledge.

* To whom correspondence should be addressed. Phone: +33(0)145523531. Fax: +33(0)145528322. E-mail: patrice.paricaud@ensta.fr.

10.1021/jp1067457
Published on Web 12/21/2010

Tetraalkylammonium halide semiclathrate hydrates have recently received much attention from both industry and researchers, as they can be used for refrigerants,[19] gas separation,[20,21] and gas storage materials.[22] In the presence of gas molecules, tetraalkylammonium halide + water systems can form gas semiclathrate hydrates: it has been found that small gas molecules can be encaged in the dodecahedral cavities of the semiclathrate hydrate.[16] While strong electrolytes such as NaCl are gas hydrate inhibitors,[23−25] tetraalkylammonium halide salts are additives that promote formation of hydrates at low pressures and near room temperature. Extensive experimental measurements of the dissociation conditions of gas semiclathrate hydrates of tetraalkylammonium salts have been performed in the past few years.[20,21,26−37] While different theoretical models have been developed for gas hydrates formed in the presence of nonelectrolyte promoters like tetrahydrofuran (THF),[38−44] no theoretical approach has ever been proposed for gas semiclathrate hydrates. One can only refer to the accurate modeling tool proposed by Mohammadi et al.[45] for hydrogen + TBAB semiclathrate hydrates, which is based on a neural network algorithm.

This work aims at proposing a thermodynamic approach to model the SLE involving salt hydrates and gas semiclathrate hydrates. An accurate prediction of SLE in electrolyte systems first requires a reliable thermodynamic model to compute the properties of electrolyte aqueous solutions. Here, we use the square-well version of the SAFT-VRE (statistical associating fluid theory with variable range for electrolytes) equation of state proposed by Galindo et al.[46] The advantage of electrolyte equations of state in comparison to electrolyte excess Gibbs energy models is the possibility to determine the properties of the liquid and vapor phases at high pressures with the same mathematical expression. As a result, electrolyte equations of state usually require fewer adjustable parameters.

This paper is organized as follows: we first discuss the SLE equilibrium conditions in electrolyte systems that involve ice and salt hydrates. We extend the methodology to gas semiclathrate hydrates by combining our approach for salt hydrates with the van de Waals−Platteeuw model[47] for gas hydrates. The main expressions of the SAFT-VRE model for electrolyte solutions are then briefly recalled. In the result section, we present the calculations obtained for HI + H_2O, LiBr + H_2O, and TBAB + H_2O binary systems and discuss the phase behavior of the TBAB + H_2O + CO_2 system.

2. Thermodynamic Approach

Let us consider an electrolyte solution at temperature T and pressure P that contains m_s moles of the salt $C_{\nu_C}A_{\nu_A}$ per kilogram of water, where C and A denote the cations and anions. We assume that the salt does not exhibit any ion pairing in solution and fully dissociates as $C_{\nu_C}A_{\nu_A} \rightarrow \nu_C C + \nu_A A$. The solid−liquid temperature−composition diagram of the electrolyte solution can exhibit different SLE regions depending on the molality m_s: in the very dilute region and for temperatures just below 0 °C, solid−liquid coexistence occurs between ice and the electrolyte aqueous solution. The equilibrium between the liquid phase and the anhydrous solid salt occurs for highly concentrated solutions. For intermediate molalities one can find several hydrates that coexist with the liquid. This work only deals with the dilute and semidilute region, i.e., the SLE for the highly concentrated region is not treated.

2.1. Solid−Liquid Equilibria between the Electrolyte Solution and Ice. Let us first consider the equilibrium between ice and the liquid phase. At a fixed pressure P, SLE is solved by imposing the equality of the chemical potential of water in ice and in the liquid phase. The chemical potential of water in the liquid phase can be expressed as $\mu_w^{liq} = \mu_w^{liq*} + kT \ln (x_w\gamma_w)$, where μ_w^{liq*} is the chemical potential of pure liquid water at T and P, x_w and γ_w are the mole fraction and activity coefficient of water, and k is the Boltzmann constant. SLE is solved by satisfying the equality $\mu_w^{ice*} = \mu_w^{liq}$, where μ_w^{ice*} is the chemical potential of pure ice at T and P. The SLE condition can then be expressed as

$$\ln(x_w\gamma_w) = -\frac{\Delta h_{mw}}{RT}\left(1 - \frac{T}{T_{mw}}\right) + \frac{\Delta c_{pw}}{R}\left(\frac{T_{mw} - T}{T}\right) - \frac{\Delta c_{pw}}{R}\ln\left(\frac{T_{mw}}{T}\right) - \frac{\Delta v_w}{RT}(P - P_0) \quad (1)$$

where T_{mw} and Δh_{mw} are the experimental melting point and molar fusion enthalpy of ice, R is the ideal gas constant, Δv_w is the difference between the molar volumes of pure liquid water and ice, and Δc_{pw} is the difference between the molar heat capacities of pure liquid water and ice. One can assume that Δc_{pw} and Δv_w are constant over the considered temperature and pressure ranges and use their experimental values at the melting point of water, i.e., $\Delta h_{mw} = 6.01$ kJ·mol^{-1}, $T_{mw} = 273.15$ K, $\Delta v_w = -1.6$ cm^3·mol^{-1}, and $\Delta c_{pw} = 40.9$ J·mol^{-1}·K^{-1}.

2.2. Solid−Liquid Equilibria between the Electrolyte Solution and Hydrate Compounds. Let us now express the SLE condition between the liquid phase and a hydrate formed from ν_w water molecules per molecule of salt $C_{\nu_C}A_{\nu_A}$. The total Gibbs energy G_{sys} of the system (solid +liquid phases) is given by

$$G_{sys} = N_w^{liq}\mu_w^{liq} + N_C^{liq}\mu_C^{liq} + N_A^{liq}\mu_A^{liq} + N_w^{hyd}\mu_w^{hyd} + N_C^{hyd}\mu_C^{hyd} + N_A^{hyd}\mu_A^{hyd} \quad (2)$$

where N_w^{liq}, N_C^{liq}, N_A^{liq} and N_w^{hyd}, N_C^{hyd}, N_A^{hyd} are the numbers of water molecules, cations, and anions in the liquid and hydrate phases, respectively, and μ_w^{liq}, μ_C^{liq}, μ_A^{liq} and μ_w^{hyd}, μ_C^{hyd}, μ_A^{hyd} are the corresponding chemical potentials. The SLE condition can be derived by expressing the differential of G_{sys}. The stoichiometry requirement for the composition of the hydrate leads to $dN_w^{liq}/\nu_w = dN_C^{liq}/\nu_C = dN_A^{liq}/\nu_A$ and $dN_w^{hyd}/\nu_w = dN_C^{hyd}/\nu_C = dN_A^{hyd}/\nu_A$. The mass balance equations between the liquid and hydrate phases lead to $dN_i^{liq} = -dN_i^{hyd}$ for all species i. As a result, the differential of G_{sys} at fixed T and P is given by

$$dG_{sys} = \frac{dN_w^{hyd}}{\nu_w}(\nu_w\mu_w^{hyd} + \nu_C\mu_C^{hyd} + \nu_A\mu_A^{hyd} - (\nu_w\mu_w^{liq} + \nu_C\mu_C^{liq} + \nu_A\mu_A^{liq})) \quad (3)$$

Since $dG_{sys} = 0$ at equilibrium and since dN_w^{hyd} can take any value, the equilibrium condition at fixed T and P is given by

$$\Delta g_{dis} = \nu_w\mu_w^{liq} + \nu_C\mu_C^{liq} + \nu_A\mu_A^{liq} - \nu_w\mu_w^{hyd} - \nu_C\mu_C^{hyd} - \nu_A\mu_A^{hyd} = 0 \quad (4)$$

where Δg_{dis} is the dissociation Gibbs free energy per molecule of salt, which is equal to 0 at equilibrium. Note that the equilibrium condition is not the equality of the chemical

potential of water in both phases, as it is for the SLE involving ice or gas hydrates. Equation 4 is similar to a chemical equilibrium and consistent with the methodology proposed by Folas et al.[48] and Tumakaka et al.[49] for SLE calculations that involve solid compounds. Note that eq 4 still holds for systems containing gas semiclathrate hydrates (eq 17). We recall that the chemical potential of chemical species i (ions or water) in the liquid phase can be expressed in the mole fraction scale as $\mu_i^{liq} = \mu_i^{ref(x)} + kT \ln(x_i\gamma_i)$, where $\mu_i^{ref(x)}$ is the reference chemical potential, γ_i the activity coefficient of chemical species i defined in the mole fraction scale, and x_i the mole fraction of chemical species i. The reference state is the infinite dilution in pure liquid water at T and P. Let us define μ^{hyd} as $\mu^{hyd} = \nu_w\mu_w^{hyd} + \nu_C\mu_C^{hyd} + \nu_A\mu_A^{hyd}$, μ^{hyd} is the Gibbs free energy of the salt hydrate phase per molecule of salt. Since the salt hydrate composition is stoichiometric (i.e., fixed), μ^{hyd} only depends on T and P. The equilibrium condition (eq 4) can be written as

$$\frac{\Delta g_{dis}}{kT} = \frac{\Delta g^0}{kT} + \nu_C \ln(x_C\gamma_C) + \nu_A \ln(x_A\gamma_A) + \nu_w \ln(x_w\gamma_w) = 0 \quad (5)$$

where the function $\Delta g^0 = \nu_w\mu_w^{liq*} + \nu_C\mu_C^{ref(x)} + \nu_A\mu_A^{ref(x)} - \mu^{hyd}$ only depends on T and P. The key to model SLE and dissociation enthalpies over a wide composition range with few adjustable parameters consists in determining Δg^0 from eq 5 at the congruent (stoichiometric) composition.[49] Let T_0 be the melting point of the hydrate at the stoichiometric composition and at atmospheric pressure $P_0 = 0.101325$ MPa. By applying eq 5 at the stoichiometric composition ($x_w^{(st)}$, $x_C^{(st)}$, $x_A^{(st)}$), one can determine $\Delta g^0(T_0,P_0)$ from the electrolyte thermodynamic model (SAFT-VRE in this study) as

$$\frac{\Delta g^0(T_0,P_0)}{kT_0} = -\nu_C \ln(x_C^{(st)}\gamma_C^{(st)}) - \nu_A \ln(x_A^{(st)}\gamma_A^{(st)}) - \nu_w \ln(x_w^{(st)}\gamma_w^{(st)}) \quad (6)$$

where $x_w^{(st)}/\nu_w = x_C^{(st)}/\nu_C = x_A^{(st)}/\nu_A = 1/(\nu_w + \nu_C + \nu_A)$. One can express Δg^0 at T and P as

$$\frac{\Delta g^0}{kT} = \frac{\Delta h^0}{kT}\left(1 - \frac{T}{T_0}\right) - \frac{\Delta c_p^0}{k}\left(\frac{T_0 - T}{T}\right) + \frac{\Delta c_p^0}{k}\ln\left(\frac{T_0}{T}\right) + \frac{\Delta v^0}{kT}(P - P_0) + \frac{\Delta g^0(T_0,P_0)}{kT_0} \quad (7)$$

where Δh^0 is an enthalpic contribution that can be adjusted on the SLE coexistence curve and dissociation enthalpy of the salt hydrate; Δc_p^0 can also be used to adjust $T-x$ diagrams, dissociation enthalpies, and heat capacities; Δv^0 is necessary to predict the effect of pressure on the melting points for the salt + water binary system. The equilibrium condition (eq 5) becomes

$$0 = \frac{\Delta g_{dis}}{kT} = \frac{\Delta h^0}{kT}\left(1 - \frac{T}{T_0}\right) - \frac{\Delta c_p^0}{k}\left(\frac{T_0 - T}{T}\right) + \frac{\Delta c_p^0}{k} \times \ln\left(\frac{T_0}{T}\right) + \frac{\Delta v^0}{kT}(P - P_0) + \frac{\Delta g^0(T_0,P_0)}{kT_0} + \nu_C \ln(x_C\gamma_C) + \nu_C \ln(x_A\gamma_A) + \nu_w \ln(x_w\gamma_w) \quad (8)$$

where $P_0 = 0.101325$ MPa. Different values for Δv^0, Δh^0, T_0, and Δc_p^0 should be used for different types of hydrates. The hydration number ν_w is fixed to its experimental value. Following the work of Folas et al.,[48] one can determine Δh^0 and T_0 by fitting the solid−liquid coexistence curves and hydrate dissociation enthalpies if the latter are available. Like in the previous section, we assume that Δv^0 is constant over the studied temperature and pressure ranges. One can assume that $\Delta c_p^0 = 0$ to reduce the number of adjusted parameters. The dissociation enthalpy Δh_{dis} of the hydrate is calculated from $\Delta h_{dis} = -T^2\partial(\Delta g_{dis}/T)/\partial T$. Although $\Delta g_{dis} = 0$ at equilibrium, the derivative of Δg_{dis} with respect to temperature T at fixed P and fixed composition is not zero and the temperature dependence of Δg_{dis} is given by eq 8. One should not confuse the dissociation enthalpy Δh_{dis} with Δh^0, although Δh^0 and Δh_{dis} have very similar values. At the congruent melting ($T = T_0$, $P = P_0$), Δh_{dis} is given by $\Delta h_{dis} = \Delta h^0 - kT^2(\partial)/(\partial T)(\nu_C \ln \gamma_C + \nu_A \ln \gamma_A + \nu_w \ln \gamma_w)$.

2.3. Thermodynamic Model for Gas Semiclathrate Hydrates. We consider a multicomponent system at temperature T and pressure P composed of $C_{\nu_C}A_{\nu_A}$ salt (for example, TBAB), water, and N_g types of gas molecules (methane, carbon dioxide, hydrogen, ...), which exhibits solid−liquid−vapor equilibrium with formation of a gas semiclathrate hydrate phase. The proposed approach is based on a combination of our model for salt hydrates (section 2.2) with the van der Waals−Platteeuw (vdW−P) model[47,50,51] for gas hydrates. The key point is to consider that the metastable empty hydrate phase β can have different structures that correspond to the different semiclathrate hydrate phases observed in the salt + H_2O binary system. For example, in the case of TBAB, one assumes that the structures of gas semiclathrate hydrates of TBAB can be of types A and B, with hydrations numbers $\nu_w = 26$ and 38, respectively. This hypothesis should be checked experimentally. However, it leads to very good predictions of the dissociation conditions of carbon dioxide semiclathrate hydrates, as shown in the results.

The semigrand partition function Ξ of the gas semiclathrate hydrate phase can be derived by using the same hypothesizes as those suggested by van der Waals and Platteeuw,[47] i.e., the positions of the host molecules (H_2O, cations, and anions) are fixed and the cavities are not distorted by the gas molecules; the cavities are assumed to be spherical and can only contain one gas molecule; the guest−guest interactions are neglected as well as quantum effects. The reader is directed to the original paper of van der Waals and Platteeuw[47] and to an alternative and rigorous derivation of the vdw−P model made by Wierzchowski and Monson.[52] To derive the semigrand partition function Ξ of the filled hydrate phase, one considers that the numbers N_w, N_C, and N_A of water molecules, cations, and anions in the hydrate phase are fixed, and the numbers N_j of gas molecules j contained in the hydrate phase can vary. Following the derivation of van der Waals and Platteeuw,[47,50] one can express Ξ as

$$\ln \Xi = -\frac{A^{\mathrm{hyd},\beta}}{kT} + N_{\mathrm{salt}} \sum_{i=1}^{N_{\mathrm{cav}}} n_i \ln\left(1 + \sum_{j=1}^{N_g} q_{ij}\lambda_j\right) \quad (9)$$

where $A^{\mathrm{hyd},\beta}$ is the Helmholtz free energy of the empty hydrate phase β, which depends on T, V, N_w, N_C, and N_A, N_{salt} is the number of salt molecules in the hydrate ($N_{\mathrm{salt}} = N_C/\nu_C = N_A/\nu_A = N_w/\nu_w$), n_i is the number of cavities of type i per salt molecule in the hydrate, N_{cav} is the number of cavity types that encage gas molecules, q_{ij} is the partition function of molecule j in cavity i, and λ_j is the absolute activity of molecule j. The differential of ln Ξ is given by[47,50]

$$-\mathrm{d}(\ln \Xi) = -S\,\mathrm{d}T - P\,\mathrm{d}V + \mu_C^{\mathrm{hyd,F}}\,\mathrm{d}N_C + \mu_A^{\mathrm{hyd,F}}\,\mathrm{d}N_A + \mu_w^{\mathrm{hyd,F}}\,\mathrm{d}N_w - \sum_{j=1}^{N_g} N_j\,\mathrm{d}\lambda_j/\lambda_j \quad (10)$$

where $\mu_C^{\mathrm{hyd,F}}$, $\mu_A^{\mathrm{hyd,F}}$, and $\mu_w^{\mathrm{hyd,F}}$ are the chemical potentials of the cations, anions, and water in the filled hydrate phase (the superscript hyd,F stands for the hydrate phase partially filled of gas molecules). Note that $N_j = \sum_{i=1}^{N_{\mathrm{cage}}} N_{ij}$, where N_{ij} is the number of gas molecules j that occupy cavities of type i. Equation 10 is different from the original van der Waals and Platteeuw[47] theory because it contains the ionic chemical potentials $\mu_C^{\mathrm{hyd,F}}$, $\mu_A^{\mathrm{hyd,F}}$. Since $N_{\mathrm{salt}} = N_C/\nu_C = N_A/\nu_A = N_w/\nu_w$ due to the stoichiometric composition of the hydrate, eq 10 can be rewritten as

$$-\mathrm{d}(\ln \Xi) = -S\,\mathrm{d}T - P\,\mathrm{d}V + (\nu_C\mu_C^{\mathrm{hyd,F}} + \nu_A\mu_A^{\mathrm{hyd,F}} + \nu_w\mu_w^{\mathrm{hyd,F}})\mathrm{d}N_{\mathrm{salt}} - \sum_{j=1}^{N_g} N_j\,\mathrm{d}\lambda_j/\lambda_j \quad (11)$$

One can define $\mu^{\mathrm{hyd,F}}$ as $\mu^{\mathrm{hyd,F}} = \nu_C\mu_C^{\mathrm{hyd,F}} + \nu_A\mu_A^{\mathrm{hyd,F}} + \nu_w\mu_w^{\mathrm{hyd,F}}$. It is clear from eqs 10 and 11 that

$$\mu^{\mathrm{hyd,F}} = -\nu_C\left(\frac{\partial \ln \Xi}{\mathrm{d}N_C}\right)_{T,V,N_w,N_A,\lambda_i} - \nu_A\left(\frac{\partial \ln \Xi}{\mathrm{d}N_A}\right)_{T,V,N_w,N_C,\lambda_i} - \nu_w\left(\frac{\partial \ln \Xi}{\mathrm{d}N_w}\right)_{T,V,N_C,N_A,\lambda_i} = -\left(\frac{\partial \ln \Xi}{\mathrm{d}N_{\mathrm{salt}}}\right)_{T,V,\lambda_i} \quad (12)$$

Since $N_j = \lambda_j \partial \ln \Xi/\partial\lambda_j$, the fraction Y_{ij} of cavities of type i occupied by gas molecules of type j is given by[47]

$$Y_{ij} = \frac{q_{ij}\lambda_j}{1 + \sum_{k=1}^{N_g} q_{ik}\lambda_k} \quad (13)$$

Equations 9, 12, and 13 lead to

$$\mu^{\mathrm{hyd,F}} = \mu^{\mathrm{hyd},\beta} + kT\sum_{i=1}^{N_{\mathrm{cav}}} n_i \ln\left(1 - \sum_{j=1}^{N_g} Y_{ij}\right) \quad (14)$$

where $\mu^{\mathrm{hyd},\beta} = \nu_w\mu_w^{\mathrm{hyd},\beta} + \nu_C\mu_C^{\mathrm{hyd},\beta} + \nu_A\mu_A^{\mathrm{hyd},\beta}$ is the Gibbs free energy per salt molecule of the empty metastable hydrate phase β. One can define the Langmuir constants C_{ij} as[53] $C_{ij} = q_{ij}\lambda_j/f_j$, where f_j is the fugacity of molecule j. It can be shown that C_{ij} only depends on T and on the cell potential. By assuming that the cavities are spherical, one can express C_{ij} as

$$C_{ij} = \frac{4\pi}{kT}\int_0^{R_{\mathrm{cav},i}} \exp\left(\frac{-w_{ij}(r)}{kT}\right) r^2\,\mathrm{d}r \quad (15)$$

where $R_{\mathrm{cav},i}$ is the effective radius of cavity i, r the distance between the gas molecule center of mass and the center of the cavity, and w_{ij} the cell potential between gas molecule j and host molecules. As shown by Barrer and Edge[54] and Parrish and Prausnitz[53] one can use a square-well (SW) potential for w_{ij}. In this case, the Langmuir constants can be expressed as

$$C_{ij} = \frac{4\pi}{kT} V_{ij}^{\mathrm{cell}} \exp\left(\frac{\varepsilon_{ij}^{\mathrm{cell}}}{kT}\right) \quad (16)$$

where V_{ij}^{cell} is the free volume of molecule j inside cavity i and $\varepsilon_{ij}^{\mathrm{cell}}$ the depth of the SW cell potential.

Liquid−vapor−hydrate three-phase equilibrium is calculated with the following procedure. At the limit of appearance of the semiclathrate hydrate phase, one can neglect the mass of the semiclathrate hydrate phase in comparison to the masses of the liquid and vapor phases. The conditions for VLE are the equality of the pressure, temperature, and chemical potentials of all species (apart from TBA^+ and Br^- ions) in the vapor and liquid phases. For given temperature, pressure, and global composition of the mixture, the VLE can be solved by performing a flash calculation that provides the compositions of the vapor and liquid phases. Finding the condition for the formation of a semiclathrate hydrate consists in finding the pressure P at which the hydrate phase first appears for given temperature and global composition. By following section 2.2 and applying the minimization criterion of the total Gibbs energy under stoichiometric constrains, one can show that the equilibrium conditions for the formation of a gas semiclathrate hydrate are the equality of the chemical potentials of the gas molecules and the following equation

$$\nu_w\mu_w^{\mathrm{liq}} + \nu_C\mu_C^{\mathrm{liq}} + \nu_A\mu_A^{\mathrm{liq}} - \nu_w\mu_w^{\mathrm{hyd,F}} - \nu_C\mu_C^{\mathrm{hyd,F}} - \nu_A\mu_A^{\mathrm{hyd,F}} = 0 \quad (17)$$

By combining eqs 7, 14, and 17 with the definition of the chemical potentials of water and the ions in the liquid phase, one can write the equilibrium condition as

$$\nu_C \ln(x_C\gamma_C) + \nu_A \ln(x_A\gamma_A) + \nu_w \ln(x_w\gamma_w) = \sum_{i=1}^{N_{\mathrm{cav}}} n_i \ln\left(1 - \sum_{j=1}^{N_g} Y_{ij}\right) - \frac{\Delta h^0}{kT}\left(1 - \frac{T}{T_0}\right) + \frac{\Delta c_p^0}{k}\left(\frac{T_0 - T}{T}\right) - \frac{\Delta c_p^0}{k}\ln\left(\frac{T_0}{T}\right) - \frac{\Delta v^0}{kT}(P - P_0) - \frac{\Delta g^0(T_0, P_0)}{kT_0} \quad (18)$$

TABLE 1: SAFT-VR Pure Component Parameters

compounds	m	σ (Å)	ε/k (K)	λ	sites	ε_{HB}/k (K)	k_{HB} (Å^3)	ref
H_2O	1	3.036	253.30	1.8000	4C model: 2H+2E	1365.92	1.0202	58,62,66
CO_2	2	3.1364	168.89	1.5157	no site			66

where, for instance, $\nu_C = \nu_A = 1$ and $\nu_w = 38$ for the TBAB·38H_2O hydrate. If several hydrate phases with different stoichiometric compositions can appear, the SLE is solved by choosing the hydrate phase having the lowest dissociation Gibbs free energy. Therefore, our model can predict a change of hydrate structure as pressure is increased, as long as the properties of the different hydrate phases (hydration numbers, T_0, ΔH^0, Δv^0) are known. Note that our approach has some similarities with the Chen-Guo model[55] for mixed-gas hydrates, which is based on a two-step mechanism for the formation of the gas hydrate phase.[55] Another model based on similar ideas has recently been proposed by Papadimitriou et al.[43] for gas + THF hydrates. However, the SLE condition in the Papadimitriou et al.[43] model is expressed in terms of the chemical potential of water, while in our approach the SLE condition is expressed in terms a stoichiometric sum of chemical potentials (eq 17).

2.4. SAFT-VRE Equation of State. The SAFT-VRE electrolyte equation of state proposed by Galindo et al.[46] is used to calculate the properties of the fluid phases. The full analytical expression of the SAFT-VRE theory can be found in refs 46 and 56−58. In the SAFT-VRE approach, molecules i are modeled as fully flexible chains of m_i tangent hard spheres of diameter σ_i while ions are modeled as charged hard spheres. The interactions between segments of type i and j are modeled with a square-well potential u_{ji} of depth ε_{ij}, diameter σ_{ij}, and range λ_{ij}. The SAFT-VRE model can be expressed as a sum of different free energy contributions

$$\frac{A}{NkT} = \frac{A^{\text{ideal}}}{NkT} + \frac{A^{\text{seg}}}{NkT} + \frac{A^{\text{chain}}}{NkT} + \frac{A^{\text{assoc}}}{NkT} + \frac{A^{\text{MSA}}}{NkT} \tag{19}$$

where A^{ideal} is the Helmholtz free energy of an ideal gas mixture, $A^{\text{seg}} = A^{\text{hs}} + A_1 + A_2$ is the segment contribution, and A^{hs} is the expression of the residual Helmholtz free energy of a hard-sphere mixture proposed by the Boublík[59] and Mansoori et al.[60] The MIX1b mixing rules[57] are used to compute the perturbation terms A_1 and A_2. A^{chain} and A^{assoc} are the chain and association contributions, respectively. The Lorentz−Berthelot combining rules are applied with a binary parameter k_{ij}, i.e.

$$\sigma_{ij} = (\sigma_{ii} + \sigma_{jj})/2, \varepsilon_{ij} = \sqrt{\varepsilon_{ii}\varepsilon_{jj}}(1 - k_{ij}) \tag{20}$$

A simple combining rule is used for the cross square-well range with another binary parameter l_{ij}, i.e.

$$\lambda_{ij} = (\sigma_{ii}\lambda_{ii} + \sigma_{jj}\lambda_{jj})(1 - l_{ij})/(\sigma_{ii} + \sigma_{jj}) \tag{21}$$

The A^{MSA} term is the MSA expression obtained by Waisman and Lebowitz[61] for the restricted primitive model (RPM). Cations and anions are represented as charged hard spheres that are immerged in a dielectric continuum of constant D. Following the work of Patel et al.[58] and Paricaud et al.,[62] we suppose that the dielectric constant D of the continuum is equal to the dielectric constant of pure saturated liquid water at temperature T. We use the correlation proposed by Paricaud et al.[62] to compute D.

The chemical potential μ_i of component i is obtained from $\mu_i = (\partial A/\partial N_i)_{T,V,N_j,j \neq i}$. The chemical potential μ_i can be written as $\mu_i = \mu_i^0 + kT \ln(\rho x_i) + \mu_i^{\text{res}}$, where μ_i^0 only depends on temperature T and μ_i^{res} is the residual part of the chemical potential. The number density ρ of the phase is numerically determined at fixed temperature, pressure, and composition. The activity coefficient γ_i of chemical species i in the mole fraction scale is determined from

$$\gamma_i = \frac{\rho}{\rho_{\text{ref}}} \exp\left(\frac{\mu_i^{\text{res}} - \mu_i^{\text{res(ref)}}}{kT}\right) \tag{22}$$

where ρ and ρ_{ref} are the number densities of the liquid phase at T, P, and in the reference state (pure liquid water at T, P), respectively, and μ_i^{res}, $\mu_i^{\text{res(ref)}}$ are the corresponding residual chemical potentials of chemical species i. The activity coefficient of ion i in the molality scale is given by[63] $\gamma_i^{(m)} = \gamma_i x_w$, where x_w is the mole fraction of water in the strong electrolyte solution. In the case of water + salt binary systems, one can calculate x_w from the salt molality m_s as $x_w = 1/(1 + 0.001(\nu_C + \nu_A)m_s M_w)$, where M_w is the molecular weight of water (18.0153 g·mol^{-1}). The mean activity coefficient of salt $C_{\nu_C}A_{\nu_A}$ is defined as $\gamma^{+-} = (\gamma_C^{(m)\nu_C}\gamma_A^{(m)\nu_A})^{1/(\nu_C + \nu_A)}$, and the osmotic coefficient is defined as[63] $\phi = -1000 \ln(x_w\gamma_w)/(m_s M_w(\nu_C + \nu_A))$. The relative apparent molal enthalpy L_ϕ is determined from[64,65] $L_\phi = (\nu_C + \nu_A)RT^2\partial(\phi - \ln \gamma^{+-})/\partial T$. The fugacity f_i of component i is given by $f_i = kT\rho x_i \exp(\mu_i^{\text{res}}/(kT))$.

2.5. Molecular Models. Water is represented as a square-well sphere of diameter $\sigma = 3.0360$ Å of range $\lambda = 1.8$ and potential depth $\varepsilon/k = 253.3$ K; hydrogen bonds between water molecules are represented by four associating sites: two donor sites H represent the hydrogen atoms, and two acceptor sites E represent the electronic pairs on the oxygen atom. The parameters for water are the same as those used in refs 58, 62, and 66. Carbon dioxide is modeled as a nonassociating compound. The SAFT-VR parameters of the pure compounds can be found in Table 1. Ions are treated as charged hard spheres of diameter σ_{ion}. We assume that the SAFT-VRE parameters of anions and cations of a given salt are equal in order to decrease the total number of parameters that characterize a salt. Thus, we use salt parameters instead of ionic parameters. Such an approach has been previously used by different authors.[62,67,68] Following the work of Galindo et al.,[46] we neglect the dispersion energy parameter ε_{ij} between ions and only consider the water−ion solvation interactions through a short-range square-well potential of range $\lambda_{\text{w-ion}}$ and depth $\varepsilon_{\text{w-ion}}$. A temperature-dependent correlation is used for the energy parameter $\varepsilon_{\text{w-ion}}$ between water and the ions, which is given by[62]

$$\varepsilon_{\text{w-ion}}/k = \varepsilon_{\text{w-ion}}^{(298)}/k + C\left(\frac{1}{T} - \frac{1}{298.15}\right) \tag{23}$$

where $\varepsilon_{\text{w-ion}}^{(298)}$ is adjusted to the thermodynamic properties (densities and activity coefficients) of the electrolyte solution

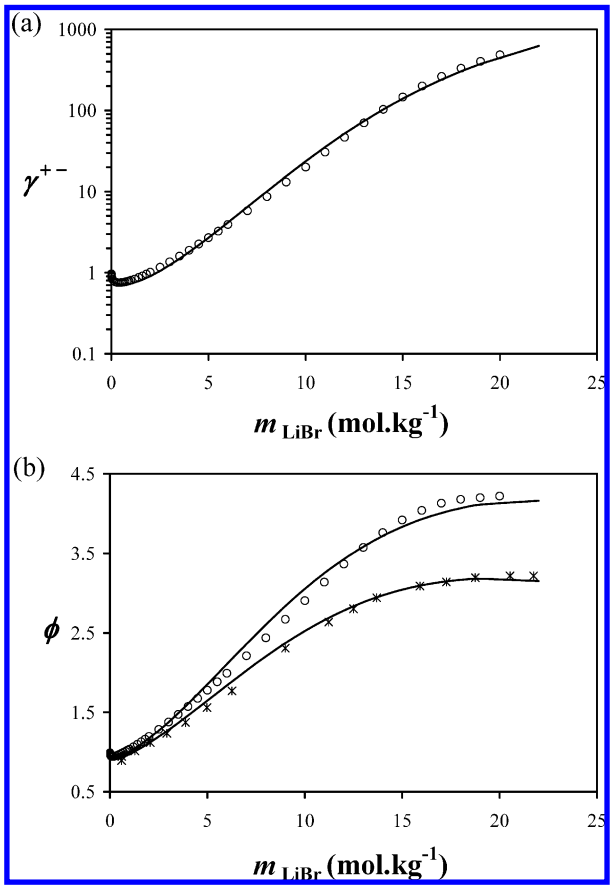

Figure 1. Thermodynamic properties of LiBr + H_2O solutions at atmospheric pressure. (a) Mean activity coefficients. (b) Osmotic coefficients. The circles denote the experimental data at $T = 298.15$K (ref 71). The asterisks correspond to a correlation of the experimental data at $T = 373.15$ K (ref 73). The solid lines correspond to the SAFT-VRE model.

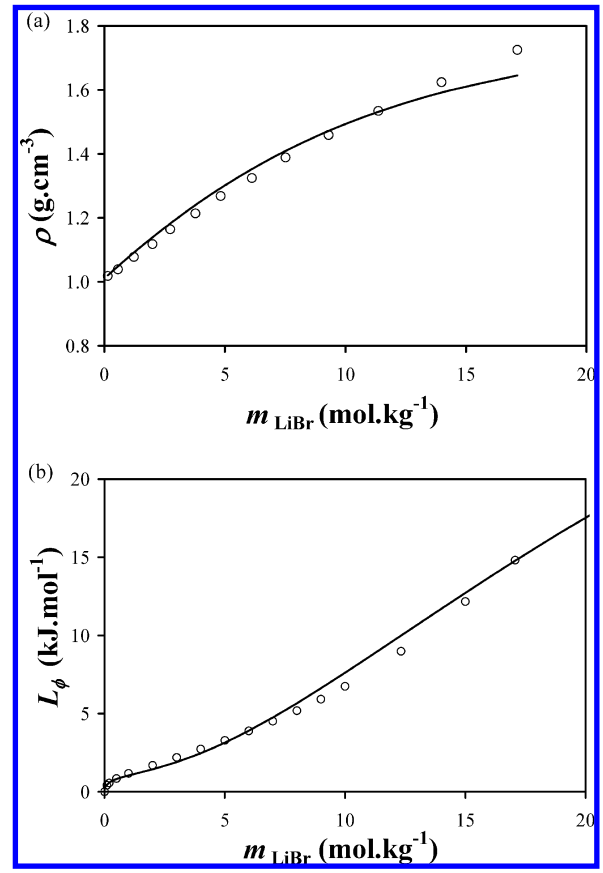

Figure 2. Thermodynamic properties of LiBr + H_2O solutions at atmospheric pressure. (a) Densities at $T = 293.15$ K. The experimental data (circles) are from ref 70. (b) Relative apparent molal enthalpies at $T = 298.15$ K. The experimental data (circles) are from Parker.[72] The solid lines correspond to the SAFT-VRE model.

at $T = 298.15$K. The C constant is very useful to model the relative apparent molal enthalpies, i.e., the effect of temperature on activity coefficients, as shown later in the Results. Note that eq 23 has previously been used to represent the VLE data of the HI−H_2O system over a broad temperature range.[62] We further assume that ion pairing does not occur in the solution. This hypothesis is not correct for highly concentrated solutions or for tetraalkymammonium salts such as TBAB, which exhibit ion pairing and clusters even at moderate concentrations.[69] However, we decided not to take this phenomenon into account to keep the approach simple and to avoid introducing more adjustable parameters (see section 3.1).

3. Results and Discussion

3.1. Thermodynamic Properties of HI, LiBr, and TBAB Aqueous Solutions. An accurate prediction of solid−liquid equilibria in aqueous electrolyte systems first requires a reliable thermodynamic model to determine the properties of the liquid phase. In particular, this thermodynamic model should accurately describe the osmotic coefficients and mean activity coefficients of the salt, as these properties are directly involved in the SLE equilibrium conditions (eqs 1, 8, and 18). The model must be accurate not only at $T = 298.15$ K but also over the temperature range of the SLE region. Here the SAFT-VRE model is used to determine the thermodynamic properties of fluid phases. The parameters for water (Table 1) are similar to those used in refs 58, 62, and 66. For the HI + H_2O system we use the salt parameters previously proposed by Paricaud et al.,[62] which were optimized on experimental densities, activity, and osmotic coefficients at $T = 298.15$ K and VLE data over a wide temperature range (see ref 62 of a detailed discussion of the properties of the HI−H_2O mixture). In this work, the salt parameters $\varepsilon^{(298)}_{w\text{-}ion}$, σ_{ion}, $\lambda_{w\text{-}ion}$, and C for LiBr have been optimized on experimental densities,[70] activity, osmotic coefficients,[71] and relative apparent molal enthalpies[72] at $T = 298.15$ K and $P = 0.101$ MPa. As shown in Figures 1 and 2, a very good description of all these properties is obtained. The average absolute deviations (AAD) between the predictions of the model and the experimental data are 1.5%, 6.9%, 2.5%, and 7.7% for densities, mean activity coefficients, osmotic coefficients, and relative apparent molal enthalpies, respectively. The osmotic coefficients of LiBr at 373.15 K (experimental data from ref 73) are also accurately predicted by the SAFT-VRE model (AAD = 3.2%). The vapor pressures of LiBr solutions have been predicted with the same parameters, and an excellent agreement with the experimental data[74,75] is obtained over wide composition and temperature ranges (Figure 3, AAD = 5.9%). In Figure 3b one can see that two data points at high temperatures for $m_{LiBr} = 17.27$ mol·kg^{-1} are clearly inconsistent with the other data.

It is well known that TBAB salt exhibits ion pairing even at moderate concentrations.[10] Since we are interesting in the dilute region, we decided not to take ion pairing into account and considered TBAB as a strong electrolyte. This approach has already been used for TBAB aqueous solutions by several authors.[9,76,77] As shown in sections 3.2 and 3.3, this hypothesis leads to accurate predictions of the SLE in the TBAB + H_2O

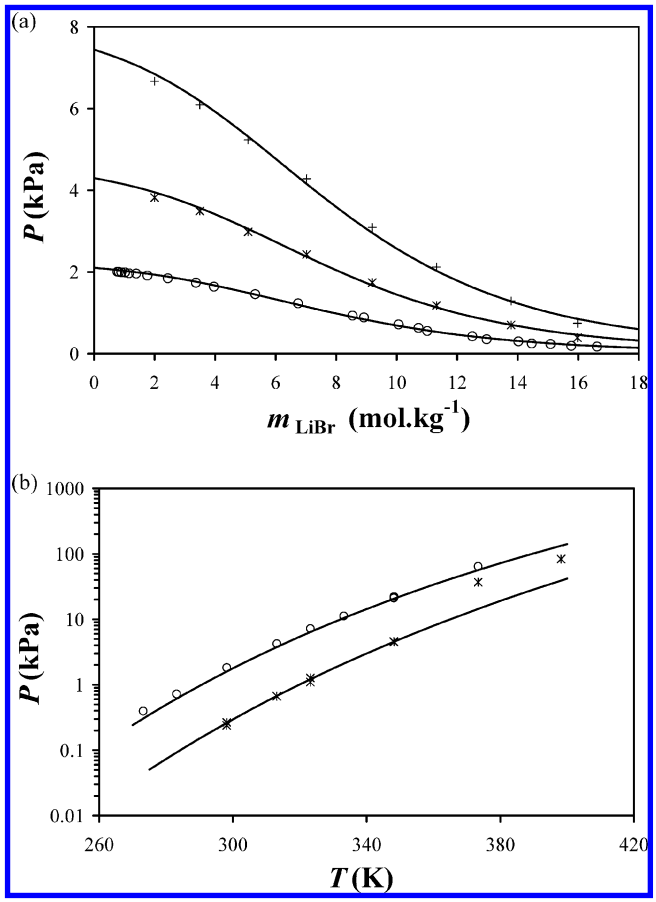

Figure 3. Vapor pressures of the LiBr + H_2O mixture. (a) Isotherms at $T = 291.15$ (circles), 303.15 (asterisks), and 313.15 K (pluses). The experimental data (symbols) are from refs 74 and 75, and the solid lines are the predictions of the SAFT-VRE model. (b) Pressure−temperature curves at different LiBr molalities: (circles) $m_{LiBR} = 7.677$ mol·kg^{-1}; (asterisks) $m_{LiBR} = 17.27$ mol·kg^{-1}. The experimental data (symbols) are from refs 74 and 75, and the solid lines correspond to the SAFT-VRE model.

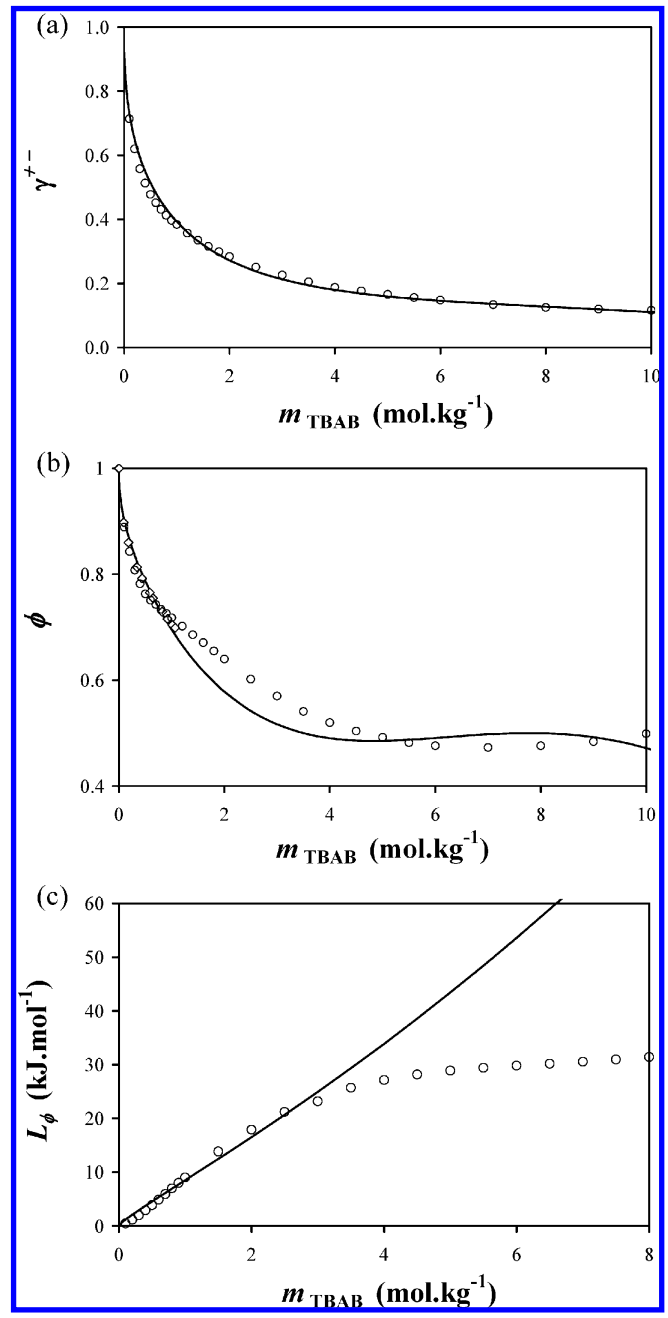

Figure 4. Thermodynamic properties of TBAB + H_2O solutions at $T = 298.15$ K and atmospheric pressure. The solid lines correspond to the predictions of the SAFT-VRE model. (a) Mean activity coefficients. (b) Osmotic coefficients. The symbols denote the experimental data (circles, ref 69; diamonds, ref 77). (c) Relative apparent molal enthalpies. The circles denote the experimental data reported in ref 79.

system. Our model may be improved by explicitly taking the formation of ion pairs into account via a chemical equilibrium.[78] However, such an approach would involve more adjustable parameters (i.e., the SAFT-VR parameters of the ion pair and the parameters for the temperature-dependent equilibrium constant), and this issue is left for future studies. The salt parameters of TBAB have been optimized on experimental mean activity coefficients and osmotic coefficients[69,77] and relative apparent molal enthalpies[79] at $T = 298.15$ K and $P = 0.101$ MPa. Density data for aqueous TBAB solutions are available[80,81] but have not been considered in the adjustment procedure. Indeed, the model overestimates the experimental densities of TBAB solutions as it cannot represent formation of low-density ice-like structures around the large hydrophobic tetra-*n*-butylammonium cations. As shown in Figure 4a and 4b, γ^{+-} and ϕ are reasonably well represented for TBAB molalities up to 10 mol·kg^{-1} (AAD = 3.9% for γ^{+-} and 4.6% for ϕ). The C constant for TBAB has been optimized on experimental relative apparent molal enthalpies at $T = 298.15$ K[69,77] for molalities up to 4.5 mol·kg^{-1}, i.e., for TBAB weight fractions up to 0.6. The absolute average deviation is about 26%. One can see in Figure 4c that the experimental relative apparent molal enthalpy L_ϕ increases as the TBAB concentration is increased in the dilute region and reaches a plateau for molalities above 4 mol·kg^{-1}. This behavior can be explained by the occurrence of ion pairing, as shown by Côté et al.[65] The salt parameters of the three salts (HI, LiBr, TBAB) are reported in Table 2.

3.2. Solid−Liquid Equilibria in HI−H_2O, LiBr−H_2O, and TBAB−H_2O Binary Systems. The thermodynamic approach described in sections 2.1 and 2.2 is employed to determine the solid−liquid coexistence curves for the HI−H_2O, LiBr−H_2O, and TBAB−H_2O systems. The SLE between ice and the liquid phase (L−ice) is predicted (no parameter adjustment) by using the salt parameters reported in Table 2. Since the temperature range of the L−ice SLE curve is wide for HI and LiBr, it is important to use the Δc_{pw} term in eq 1. Excellent predictions of the L−ice coexistence curves can be obtained for the three electrolyte systems, as shown in Figures 5−7. This confirms that the water activity is accurately predicted

TABLE 2: SAFT-VRE Salt Parameters for Hydrogen Iodide, Lithium Bromide, and Tetra-*n*-butylammonium Bromide[a]

Salts	σ_{ion}(Å)	$\varepsilon^{(298)}_{w\text{-}ion}/k$ (K)	C (K^2)	$\lambda_{w\text{-}ion}$	ref
HI	3.27	836.67	-1.4894×10^5	1.165	62
LiBr	3.269	816.90	-1.2×10^5	1.15	this work
TBAB	3.854	596.0	6.0×10^5	1.1	this work

[a] The parameters for HI were taken from ref 62. The parameters for LiBr were fitted to experimental mean activity coefficients, relative apparent molal enthalpies, osmotic coefficients, and densities. The parameters for TBAB were fitted to mean activity coefficients, osmotic coefficients, and relative apparent molal enthalpies.

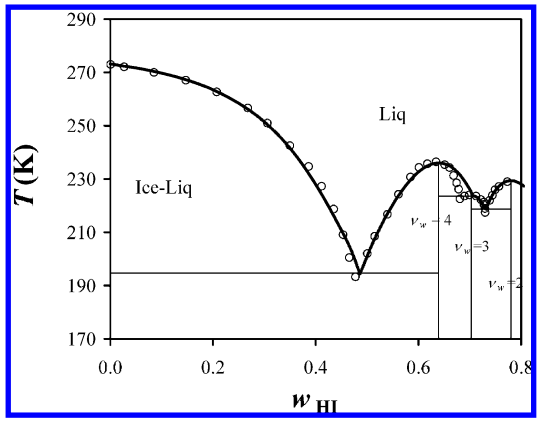

Figure 5. Temperature−composition diagram of the HI + H_2O mixture. The circles represent the experimental solid−liquid coexistence curves (refs 82 and 83). The liquid composition is expressed in terms of the HI weight fraction (w_{HI}). The solid thick lines represent the SLE curves calculated from eq 1 or 8. The thin lines denote the calculated eutectic temperatures and congruent compositions.

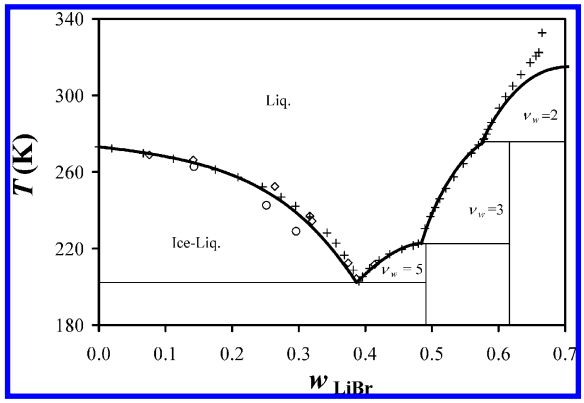

Figure 6. Temperature−composition diagram of the LiBr + H_2O mixture. The liquid composition is expressed in terms of the LiBr weight fraction (w_{LiBr}). The symbols denote the experimental data (see ref 1 for a review of experimental data). The solid thick lines represent the SLE curves calculated from eq 1 or 8, and the thin lines denote the calculated eutectic temperatures and congruent compositions. The diamonds denote Steudemann's experimental data,[84] and the circles represent the experimental data from Jones and Getman.[85] The pluses correspond to the correlations proposed by Pátek and Klomfar.[1]

by the SAFT-VRE model. The AAD between the experimental[1,82−85] and the predicted salt weight fractions in the liquid phase at fixed temperature and pressure is about 2.1% for HI and 3.6% for LiBr.

The SLE coexistence curves involving hydrate phases have been determined from eq 8 for the three-electrolyte systems. The regressed hydrate parameters are provided in Tables 3−5. A very good agreement between the experimental data[1,82,83] and

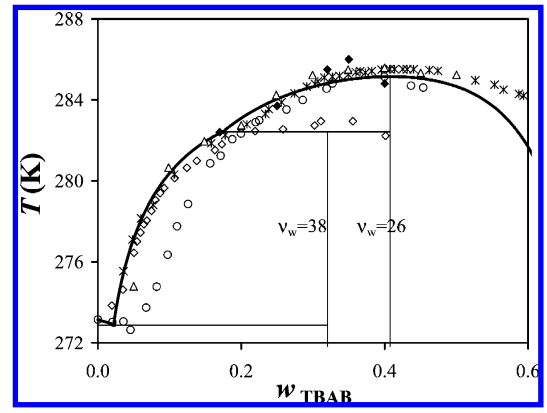

Figure 7. Temperature−composition diagram of the TBAB + H_2O mixture. The liquid composition is expressed in terms of the TBAB weight fraction (w_{TBAB}). The symbols denote the experimental data (see refs 29 and 32 for a review of experimental data): (asterisks) ref 86; (open diamonds) type A from ref 12; (circles) type B from ref 12; (pluses) hydrate with $\nu_w = 3$ from ref 86; (filled diamonds) ref 32; (open triangles) ref 87. The solid thick lines represent the SLE curves calculated from eq 1 or 8, and the thin lines denote the calculated eutectic temperatures and congruent compositions.

TABLE 3: Hydrate Parameters Used To Compute the Solid−Liquid Equilibria of the HI + H_2O System at Atmospheric Pressure[a]

ν_w	T_0 (K)	Δh^0 (kJ·mol^{-1})
4	236.0	24
3	223.9	16
2	229.4	21

[a] ν_w is the hydration number, T_0 the congruent melting point, and Δh^0 the enthalpic term used in eq 8. T_0 and Δh^0 were fitted to $T-x$ data.

TABLE 4: Hydrate Parameters Used To Compute the Solid−Liquid Equilibria of the LiBr + H_2O System at Atmospheric Pressure[a]

ν_w	T_0 (K)	Δh^0 (kJ·mol^{-1})
5	223	18.0
3	280	8.2
2	315	3.0

[a] ν_w is the hydration number, T_0 the congruent melting point, and Δh^0 the enthalpic term used in eq 8. T_0 and Δh^0 were fitted to $T-x$ data.

the model can be obtained for the HI + H_2O and LiBr + H_2O systems by adjusting only two parameters T_0 and $\Delta > h^0$ for each hydrate, as shown in Figure 6. It was assumed that $\Delta c_p^0 = 0$ to reduce the number of adjusted parameters. Three different hydrates H_4, H_3, and H_2 of hydration numbers 4, 3, and 2 are considered for the HI + H_2O system. The solid−liquid phase diagram is limited to HI weight fractions up to about 0.8 as liquid−liquid demixing occurs for higher HI concentrations. The calculated L−ice−H_4 triple point (eutectic point) for the HI + H_2O system is very close to the experimental point and located at $w_{HI} = 0.486$ and $T = 194.5$ K. In the case of the LiBr + H_2O system, there is no liquid−liquid immiscibility and four hydrates H_5, H_3, H_2, and H_1, are found experimentally.[1] In this work, the SLE curves have been calculated only for the hydrates H_5, H_3, and H_2 as the SAFT-VRE model is not applicable for highly concentrated solutions. As shown in Figure 7, a very good description of the SLE curves is obtained for H_5 and H_3 hydrates. However, the predictions are less satisfactory for the H_2 hydrate, for LiBr weight fractions $w_{LiBr} > 0.63$ (i.e., $m_{LiBr} > 20$ mol·kg^{-1}). This is due to the fact that the activity coefficients

TABLE 5: Hydrate Parameters Used To Compute the Solid−Liquid Equilibria of the TBAB + H_2O System at Atmospheric Pressure[a]

type	ν_w	T_0 (K)	Δh^0 (kJ·mol^{-1})	Δv^0 (cm^3·mol^{-1})	n_i	V_{ij}^{cell} (Å^3)	$\varepsilon_{ij}^{cell}/k$ (K)
B	38	283.50	200.7	−30	3	0.012415	2882
A	26	285.15	150.2	−30	2	0.006208	2882

[a] ν_w is the hydration number, T_0 the congruent melting point, and Δh^0 the enthalpic term expressed in kJ/mol of TBAB; Δv^0 is expressed in cm^3/mol of TBAB; n_i is the number of cavities of type i per TBAB molecule in the hydrate. The SW cell potential parameters $V_{ij}^{cell}$and ε_{ij}^{cell} for carbon dioxide are also reported. T_0, Δh^0, and Δv^0 were fitted to $T-x$ and dissociation enthalpy data.

are not well predicted at such high concentrations. The predicted L−ice−H_5 eutectic point is very close to the experimental point and located at $w_{LiBr} = 0.387$ and $T = 202.2$ K.

As discussed earlier in this paper, the solid−liquid phase behavior of the TBAB + H_2O mixture is complex and the structures and hydration numbers of the different hydrates are still not perfectly known. Several authors have suggested the existence of different hydrates varying in structure and hydration number: Dyadin and co-workers[11,86] found four different hydrates, H_{36}, H_{32}, H_{26}, and H_{24}, for TBAB weight fractions inferior to 0.6, while Shimada and co-workers[12,16−18] found two hydrates H_{26} and H_{38} denoted as type A and type B, respectively. Numerous SLE data from different sources are available for the TBAB + H_2O system[11,12,18,29,32,86−88] for TBAB weight fractions below 0.5. One can first observe (Figure 7) that the temperature range of the SLE curves for $w_{TBAB} < 0.5$ is very narrow (from 272.8 to 285 K) compared to the HI + H_2O and LiBr + H_2O systems. For the sake of simplicity, we decided to consider only two types of hydrates: H_{26} type A and H_{38} type B hydrates. The parameters T_0 and Δh^0 of both hydrates have been optimized on temperature−composition data and dissociation enthalpies and are reported in Table 5. The congruent melting point of H_{26} was set to the experimental value obtained by Oyama et al.[12] ($T_0 = 285.15$ K), while the congruent melting point (metastable) of H_{38} was fixed to 283.5 K. As shown in Figure 7, the new model accurately describes the SLE data at atmospheric pressure for TBAB weight fractions up to 0.5. The triple point (L−H_{26}−H_{38}) is predicted at $T = 282.4$ K, $w_{TBAB} = 0.174$. For TBAB weight fractions over 0.4, one can observe in Figure 7 that the experimental dissociation temperatures obtained by Lipkowski et al.[86] are slightly higher than those obtained by Oyama et al.[12] The calculated dissociation enthalpies are equal to 193.02 J·g^{-1} for type A hydrate at the congruent composition ($w_{TBAB} = 0.4077$) and 199.17 J·g^{-1} for type B hydrate at the triple-point composition ($w_{TBAB} = 0.174$). These values are close to the experimental data[12] (193.18 and 199.59 J·g^{-1}). The parameter $\Delta v^0 = -30$ cm^3/mol of TBAB for type B hydrate (H_{38}) has been optimized on the experimental dissociation temperatures at different pressures reported by Arjmandi et al.[29] A very good agreement between the new model and the experimental data is obtained, as shown in Figure 8. Since there is no such data for type A hydrate (H_{26}), the same parameter $\Delta v^0 = -30$ cm^3·mol^{-1} has been used for both type A and type B hydrates (Table 5).

3.3. Phase Behavior of the TBAB + H_2O + CO_2 System. Before modeling the dissociation conditions of CO_2 + TBAB semiclathrate hydrates, one must make sure that the thermodynamic properties of TBAB + H_2O + CO_2 fluid phases are well represented by the SAFT-VRE model. Different sets of SAFT-VR parameters have been proposed in the literature for the H_2O + CO_2 binary mixture.[66,89,90] Here, we use the parameters proposed by Valz et al.,[66] which were optimized on VLE data at temperatures and pressures close to the state conditions of interest. The effect of TBAB on the solubility of CO_2 in the liquid phase can be predicted by assuming that the dispersion interactions between the ions (TBA^+, Br^-) and CO_2 are negligible. Such an assumption was made by Patel et al.[58] to predict the salting out effect on the solubility of hydrocarbons in water. Let us consider a TBAB aqueous solution with a given initial TBAB weight fraction w_{TBAB}. The solubility of CO_2 can be determined with the SAFT-VRE model by performing a flash calculation at T, P, and fixed global mole fractions z_i. Since the water content in the vapor phase is very small, the solubility of CO_2 does not depend on the global mole fraction of CO_2 z_{CO2} but only on T, P, and the initial mole fraction ratio $z_{TBAB}/z_w = M_w/M_{TBAB} \times w_{TBAB}/(1 - w_{TBAB})$. As shown in Figure 9, the predictions of CO_2 solubilities with the SAFT-VRE model are in excellent agreement with the experimental data both for the binary H_2O + CO_2 binary mixture (experimental data from ref 91) and the H_2O+CO_2+TBAB ternary system (exp. data from ref.[30]). The deviations between the predicted CO_2 mole fractions, and the experimental data at $T = 283.15$ K and pressures up to 2.5 MPa are 5.8% for the H_2O + CO_2 binary mixture and 1.6% for the H_2O + CO_2 + TBAB ternary.

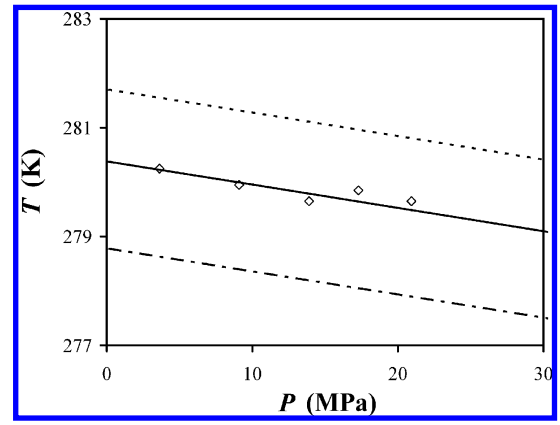

Figure 8. Effect of pressure on the dissociation temperature of the type B semiclathrate hydrate ($\nu_w = 38$) for the H_2O + TBAB binary system. The diamonds denote the experimental data of Arjmandi et al.[29] for $w_{TBAB} = 0.1$ in the initial liquid phase, and the solid line represents the predictions of the new model at the same liquid composition. The dotted and dash-dotted lines represent the predictions of the model for $w_{TBAB} = 0.14$ and 0.07, respectively.

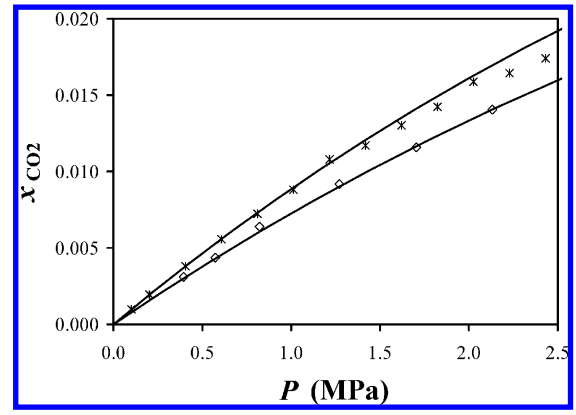

Figure 9. Solubility of carbon dioxide (VLE) in aqueous TBAB solutions at $T = 283.15$ K. The solid lines are the predictions of the SAFT-VRE model, and the symbols denote the experimental data: (asterisks) $w_{TBAB} = 0$, ref 91; (diamonds) $w_{TBAB} = 0.09$, ref 30.

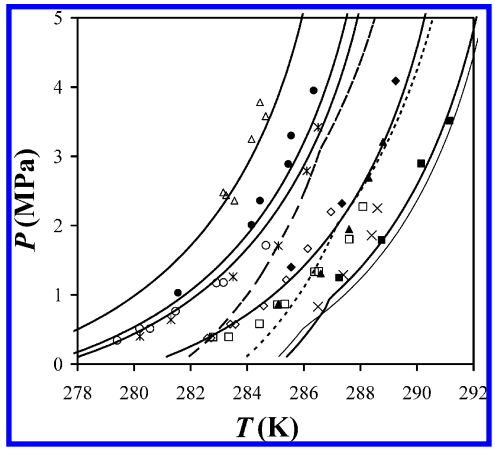

Figure 10. Liquid−vapor−hydrate (L−V−H) three-phase lines for the CO_2 + TBAB + H_2O system. The symbols denote the experimental data at different TBAB weight fractions: (open triangles) $w_{TBAB} = 0.03$, ref 31; (filled circles) $w_{TBAB} = 0.045$, ref 31; (asterisks) $w_{TBAB} = 0.05$, ref 92; (filled triangles) $w_{TBAB} = 0.1$, ref 92; (open circles) $w_{TBAB} = 0.0442$, ref 30; (open diamonds) $w_{TBAB} = 0.07$, ref 30; (open squares) $w_{TBAB} = 0.0901$, ref 30; (filled diamonds) $w_{TBAB} = 0.1$, ref 29; (filled squares) $w_{TBAB} = 0.427$, ref 29; (crosses) $w_{TBAB} = 0.4$, ref 32. The thick solid lines, from the left to the right, are the curves predicted by the new model (eq 18) at $w_{TBAB} = 0.03$, 0.045, 0.05, 0.1, and 0.427. The thin solid line is the predicted curve at $w_{TBAB} = 0.32$ (stoichiometric composition of type B hydrate). The dotted line is the predicted curve at $w_{TBAB} = 0.55$, and the long dashed curve is the predicted curve at $w_{TBAB} = 0.6$.

The liquid−vapor−semiclathrate hydrate (L−V−H) three-phase lines of the TBAB + H_2O + CO_2 ternary system have been determined by adjusting the parameters V_{ij}^{cell} and ε_{ij}^{cell} of the square-well cell potential for CO_2 on experimental dissociation pressures. First, one can observe some significant discrepancies between the experimental data from different authors at the same TBAB weight fractions (Figure 10). For instance, the dissociation pressures measured by Lin et al.[30] are lower than those measured by Arjmandi et al.[29] and H. Oyama et al.[31] As a result, we decided to fit the cell potential parameters on the data from refs 29, 31, and 92. The procedure used for three-phase equilibrium calculation is explained in great detail in section 2.3. It is assumed that the CO_2 + TBAB semiclathrate hydrates have similar structures and hydration numbers as the semiclathrate hydrates encountered in the TBAB + H_2O binary mixture, i.e., the CO_2 + TBAB semiclathrate hydrates can be of either of type A ($\nu_w = 26$) or type B ($\nu_w = 38$). According to Shimada et al.,[17] the ideal unit cell of type B TBAB semiclathrate hydrate is composed of two TBA^+ cations, two Br^- anions, 76 water molecules, and exhibits six dodecahedral cages that can encage gas molecules. As a result, the number n_i of dodecahedral cages i per TBAB molecule is set to 3 for type B hydrate. It is assumed that type A hydrate only exhibits two dodecahedral cages per TBAB molecule; thus, type B hydrate is supposed to store more CO_2 molecules per TBAB molecule than type A hydrate at high pressures. At fixed temperature, the model can accurately describe the dissociation pressures over a wide TBAB composition range ($0.03 \le w_{TBAB} \le 0.427$). Two different sets of cell potential parameters are used for types A and B: the same value for ε_{ij}^{cell} was used for both types, while different values for V_{ij}^{cell} are used for type B (Table 5). Our cell potential parameters ($A_{cell} = 4\pi V_{ij}^{cell}/k = 1.13 \times 10^{-3}$ K·MPa^{-1}, $B_{cell} = 2882$ K) have the same orders of magnitude as those found by Munk et al.[93] for the Langmuir constant of CO_2 in small cavities of structure II ($A_{cell} = 8.34 \times 10^{-4}$ K·MPa^{-1}, $B_{cell} = 3615$ K). The average deviation (AAD) between the calculated dissociation pressures and the experimental data from refs 29, 31, and 92 is 10.5%.

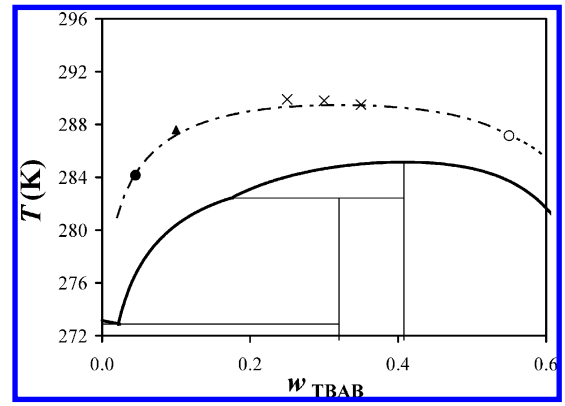

Figure 11. Temperature−composition diagrams of the TBAB + H_2O and TBAB + H_2O + CO_2 mixtures. The lines represent the predictions of the new model: the solid lines are the calculated $T-x$ diagram of the TBAB + H_2O binary mixture at atmospheric pressure. The dash-dotted line is the predicted L−V−H_{38} three-phase line at $P = 2$ MPa for type B hydrate ($\nu_w = 38$). The dotted line is the predicted L−V−H_{26} three-phase line at $P = 2$ MPa for type A hydrate ($\nu_w = 26$). The open circle denotes the predicted L−V−H_{38}−H_{26} quadruple point. The filled black circle and filled triangle denote experimental points for $w_{TBAB} = 0.045$ (ref 31) and $w_{TBAB} = 0.1$ (ref 92), respectively. The crosses denote the experimental points of Deschamps and Dalmazzone.[32]

As shown in Figure 11, the temperature−composition diagram at $P = 2$ MPa is very well predicted by the new model. The model predicts that type B is more stable than type A in the presence of CO_2 at pressures above 1 MPa. The change of structure from type A to type B is due to the fact that type B hydrate can encage more CO_2 molecules than type A hydrate; as a result, type B hydrate is more stabilized by CO_2 than type A hydrate at high pressures. In Figure 10, one can observe a break in the three-phase line for $w_{TBAB} = 0.427$ at a pressure of around 0.94 MPa, which indicates a change of structure from type A to type B. This point is a quadruple point (L−V−H_{38}−H_{26}). As the TBAB weight fraction is increased (see the three-phase lines at $w_{TBAB} = 0.55$ and 0.6), the predicted L−V−H_{38}−H_{26} quadruple point is shifted to higher pressures. A similar change of hydrate structure has been experimentally observed for semiclathrate hydrates of tetra-*n*-butyl ammonium chloride + methane (see Figure 2 of ref 34). Such a break in the three-phase curve has not been observed experimentally for the TBAB + CO_2 system; however, the amount of experimental points for these systems at $w_{TBAB} = 0.427$ and pressures close to 1 MPa is too small to observe such a change. However, in the temperature−composition diagram measured by Deschamps and Dalmazzone[32] for different gas + TBAB semiclathrate hydrates, one can clearly see that the maximum dissociation temperature at pressures above 2 MPa is around $w_{TBAB} = 0.25$ for all the studied gases, which is closer to the congruent composition of type B hydrate ($w_{TBAB} = 0.32$) than that of type A ($w_{TBAB} = 0.407$). Thus, these data seem to indicate that the hydration number of the gas semiclathrate hydrate is higher than 26, which is in agreement with our finding. The change of structure from type A to type B at high pressure can be discussed from the model and is based on a balance between the van der Waals−Platteeuw term and all other terms in eq 18. At low gas pressures, the other terms dominate and type A hydrate is stable like for the TBAB + H_2O binary system. As the gas pressure is increased, the occupied fractions Y_{ij} increase. As a result, the van der Waals−Platteeuw term becomes more and more negative and stabilizes the hydrate phase. The van der Waals−Platteeuw term of type B hydrate decreases faster than that of type A hydrate because type B has more small cages

per salt molecule ($n_i = 3$) and the Langmuir constant is larger. As a result, type B hydrate is stable at high pressure.

Another interesting behavior observed experimentally[30] is predicted by the new model. For TBAB weight fractions w_{TBAB} inferior to about 0.32, the model predicts that an increase of w_{TBAB} leads to a stabilization of type B gas semiclathrate hydrate. However, for $w_{TBAB} > 0.32$, it is predicted that type B gas semiclathrate hydrate is destabilized by an increase of w_{TBAB}. This change of behavior can be explained by the parabolic shape of the SLE curves in the $T-x$ diagram of the TBAB + H_2O binary system: at a fixed pressure, the dissociation temperature of the gas semiclathrate is lower if the dissociation temperature of the semiclathrate hydrate without gas is lower. In Figure 10 one can observe that the three-phase line for $w_{TBAB} = 0.6$ crosses the three-phase line $w_{TBAB} = 0.1$ at temperatures around 282.7 K. Duc et al.[20] found that the dissociation pressures for $w_{TBAB} = 0.65$ and 0.05 are almost equal (~0.82 MPa) at $T = 284$ K and suggested that the TBAB concentration of the initial TBAB solution may not influence the dissociation pressures. Lin et al.[30] suggested that the dissociation pressure of the gas semiclathrate hydrate changes dramatically with w_{TBAB} and is lower for w_{TBAB} close of the stoichiometric composition of the hydrate. The prediction of the new model is in agreement with the Lin et al.[30] suggestion. As shown in Figure 10, the predicted dissociation pressures of type B hydrate at $w_{TBAB} = 0.32$ (thin solid line) are lower than those at $w_{TBAB} = 0.427$ (thick solid line). However, the dissociation pressures of type A hydrate at $w_{TBAB} = 0.32$ are above those at $w_{TBAB} = 0.427$.

IV. Conclusions

A thermodynamic approach is proposed to determine the solid−liquid equilibria and dissociation conditions of hydrates in electrolyte systems. The SAFT-VRE electrolyte equation of state is employed to compute the properties of electrolyte solutions, and an accurate description of vapor pressures, relative apparent enthalpies, mean activity coefficients, and osmotic coefficients is obtained. The model has been applied to different salt systems (HI−H_2O, LiBr−H_2O, and TBAB−H_2O), and an excellent description of the SLE coexistence curves can be obtained over a wide composition range by regressing two parameters T^0 and Δh^0 on the $T-x$ diagram and dissociation enthalpy data. A new theoretical model based on a combination of the van der Waals−Platteeuw theory[47] and our approach for salt hydrates has been developed to determine the dissociation conditions of gas semiclathrate hydrates. A very good description of the liquid−vapor−semiclathrate hydrate three-phase lines of the TBAB + CO_2 + H_2O system is obtained. At high TBAB weight fractions, the new model predicts a change of hydrate structure from type A to type B as pressure is increased. Moreover, for initial TBAB concentrations above the stoichiometric composition, it is predicted that an increase of the initial TBAB weight fraction leads to a destabilization of the semiclathrate hydrate phase, while the opposite behavior is observed at low initial TBAB concentrations.

Although our approach has only been applied to the TBAB + CO_2 + H_2O system, it could be easily extended to gas mixtures and to other tetraalkymammonium salts. However, development of a thermodynamic model for a given tetraalkymammonium salt + water + gas system is a step by step procedure that requires the use of specific experimental data, such as activity coefficients and dilution enthalpies in the electrolyte solution, SLE temperature−composition curves for the different hydrates in the salt + water binary system, dissociation enthalpies, gas solubilities in pure water and in the electrolyte aqueous solution, dissociation pressures of the gas semiclathrate hydrates over a wide salt composition range, and experimental hydrate structures. Thus, the measurements of all these properties are strongly encouraged for development of a reliable model.

Acknowledgment. I thank J. Deschamps for his insightful contribution to this work. I am also grateful to D. Dalmazzone, W. Fürst, W. Bouchafaa, A. H. Mohammadi, and A. Eslamimanesh for helpful discussions.

References and Notes

(1) Pátek, J.; Klomfar, J. *Fluid Phase Equilib.* **2006**, *250*, 138–149.
(2) Stokes, R. H.; Robinson, R. A. *J. Am. Chem. Soc.* **1948**, *70*, 1870–1878.
(3) Zeng, D.; Voigt, W. *CALPHAD* **2003**, *27*, 243–251.
(4) Marcus, Y. *J. Solution Chem.* **2005**, *34*, 307–315.
(5) Wang, P.; Anderko, A.; Young, R. D. *Fluid Phase Equilib.* **2002**, *203*, 141–176.
(6) Davidson, D. W. Clathrate Hydrates. In *Water, a comprehensive treatise*; Franks, F., Ed.; Plenium Press: New York, 1973; Vol. 2 (Water in crystalline hydrates; aqueous solutions of simple nonelectrolytes), pp 140−146.
(7) Fowler, D. L.; Loebenstein, W. V.; Pall, D. B.; Kraus, C. A. *J. Am. Chem. Soc.* **1940**, *62*, 1140–1142.
(8) Kurzin, A. V.; Evdokimov, A. N.; Antipina, V. B.; Pavlova, O. S. *J. Chem. Eng. Data* **2009**, *54*, 1049–1051.
(9) Weingärtner, H.; Klante, D.; Schneider, G. M. *J. Solution Chem.* **1999**, *28*, 435–446.
(10) Slusher, J. T.; Cummings, P. T. *J. Phys. Chem. B* **1997**, *101*, 3818–3826.
(11) Dyadin, Y. A.; Udachin, K. A. *J. Inclusion Phenom.* **1984**, *2*, 61–72.
(12) Oyama, H.; Shimada, W.; Ebinuma, T.; Kamata, Y.; Takeya, S.; Uchida, T.; Nagao, J.; Narita, H. *Fluid Phase Equilib.* **2005**, *234*, 131–135.
(13) Marcus, Y. *J. Solution Chem.* **2008**, *37*, 1071–1098.
(14) Aladko, L. S.; Dyadin, Y. A.; Rodionova, T. V.; Terekhova, I. S. *J. Mol. Liq.* **2003**, *106*, 229–238.
(15) Nakayama, H. *Bull. Chem. Soc. Jpn.* **1981**, *54*, 3717–3722.
(16) Shimada, W.; Ebinuma, T.; Oyama, H.; Kamata, Y.; Takeya, S.; Uchida, T.; Nagao, J.; Narita, H. *Jpn. J. Appl. Phys.* **2003**, *42*, L129–L131.
(17) Shimada, W.; Shiro, M.; Kondo, H.; Takeya, S.; Oyama, H.; Ebinuma, T.; Narita, H. *Acta Crystallogr.* **2005**, *C61*, o65–o66.
(18) Shimada, W.; Ebinuma, T.; Oyama, H.; Kamata, S.; Narita, H. *J. Cryst. Growth* **2005**, *274*, 246–250.
(19) Zhang, Y.; Zhou, J.; Wang, Z.; Liu, J.; Cen, K. *Int. J. Hydrogen Energy* **2008**, *33*, 2211–2217.
(20) Duc, N. H.; Chauvy, F.; Herri, J.-M. *Energy Convers. Manage.* **2007**, *48*, 1313–1322.
(21) Li, S.; Fan, S.; Wang, J.; Lang, X.; Liang, D. *J. Nat. Gas Chem.* **2009**, *18*, 15–20.
(22) Strobel, T. A.; Hester, K. C.; Koh, C. A.; Sum, A. K.; Sloan, E. D. *Chem. Phys. Lett.* **2009**, *478*, 97–109.
(23) Vu, V. Q.; Suchaux, P. D.; Fürst, W. *Fluid Phase Equilib.* **2002**, *194*, 361–370.
(24) Masoudi, R.; Tohidi, B.; Danesh, A.; Todd, A. C. *Fluid Phase Equilib.* **2004**, *215*, 163–174.
(25) Ruffine, L.; Trusler, J. P. M. *J. Chem. Thermodyn.* **2010**, *42*, 605–611.
(26) Kamata, Y.; Yamakoshi, Y.; Ebinuma, T.; Oyama, H.; Shimada, W.; Narita, H. *Energy Fuels* **2005**, *19*, 1717–1722.
(27) Hashimoto, S.; Murayama, S.; Sugahara, T.; Sato, H.; Ohgaki, K. *Chem. Eng. Sci.* **2006**, *61*, 7884–7888.
(28) Li, D. L.; Du, J.-W.; Fan, S.-S.; Liang, D.-Q.; Li, X.-S.; Huang, N.-S. *J. Chem. Eng. Data* **2007**, *52*, 1916–1918.
(29) Arjmandi, M.; Chapoy, A.; Tohidi, B. *J. Chem. Eng. Data* **2007**, *52*, 2153–2158.
(30) Lin, W.; Delahaye, A.; Fournaison, L. *Fluid Phase Equilib.* **2008**, *264*, 220–227.
(31) Oyama, H.; Ebinuma, T.; Nagao, J.; Narita, H. Phase behaviour of TBAB semiclathrate hydrate crystal under several vapor components. *6th International Conference on Gas Hydrates (ICGH 2008)*, Vancouver, Canada, 2008.
(32) Deschamps, J.; Dalmazzone, D. *J. Therm. Anal. Calorim.* **2009**, *98*, 113–118.
(33) Hashimoto, S.; Tsuda, T.; Ogata, K.; Sugahara, T.; Inou, Y.; Ohgaki, K. *J. Thermodyn.* **2010**, *2010*, 170819.

(34) Makino, T.; Yamamoto, T.; Nagata, K.; Sakamoto, H.; Hashimoto, S.; Sugahara, T.; Ohgaki, K. *J. Chem. Eng. Data* **2010**, *55*, 839–841.
(35) Li, X.-S.; Xia, Z.-M.; Chen, Z.-Y.; Yan, K.-F.; Li, G.; Wu, H.-J. *J. Chem. Eng. Data* **2010**, *55*, 2180–2184.
(36) Mohammadi, A. H.; Richon, D. *J. Chem. Eng. Data* **2010**, *55*, 982–984.
(37) Mayoufi, N.; Dalmazzone, D.; Fürst, W.; Delahaye, A.; Fournaison, L. *J. Chem. Eng. Data* **2010**, *55*, 1271–1275.
(38) Delahaye, A.; Fournaison, L.; Marinhas, S.; Chatti, I.; Petitet, J.-P.; Dalmazzone, D.; Fürst, W. *Ind. Eng. Chem. Res.* **2006**, *45*, 391–397.
(39) Martinez, M. C.; Dalmazzone, D.; Fürst, W.; Delahaye, A.; Fournaison, L. *AIChE J.* **2008**, *54*, 1088–1095.
(40) Martìn, A.; Peters, C. J. *J. Phys. Chem. B* **2009**, *113*, 7548–7557.
(41) Martìn, A.; Peters, C. J. *J. Phys. Chem. B* **2009**, *113*, 7558–7563.
(42) Strobel, T. A.; Koh, C. A.; Sloan, E. D. *Fluid Phase Equilib.* **2009**, *280*, 61–67.
(43) Papadimitriou, N. I.; Tsimpanogiannis, I. N.; Stubos, A. K. *J. Chem. Phys.* **2009**, *131*, 044102.
(44) Deschamps, J.; Dalmazzone, D. *J. Chem. Eng. Data* **2010**, *55*, 3395–3399.
(45) Mohammadi, A. H.; Belandria, V.; Richon, D. *Chem. Eng. Sci.* **2010**, *65*, 4302–4305.
(46) Galindo, A.; Gil-Villegas, A.; Jackson, G.; Burgess, A. N. *J. Phys. Chem. B* **1999**, *103*, 10272–10281.
(47) van der Waals, J. H.; Platteeuw, J. C. *Adv. Chem. Phys.* **1959**, *2*, 1–57.
(48) Folas, G. K.; Gabrielsen, J.; Michelsen, M. L.; Stenby, E. H.; Kontogeorgis, G. M. *Ind. Eng. Chem. Res.* **2005**, *44*, 3823–3833.
(49) Tumakaka, F.; Prikhodko, I. V.; Sadowski, G. *Fluid Phase Equilib.* **2007**, *260*, 98–104.
(50) Sloan, E. D. *Clathrate hydrates of natural gases*, 2nd ed.; Taylor & Francis: New York, 1998.
(51) Carroll, J. *Natural gase hydrates: a guide for engineers*; GPP: Amsterdam, 2003.
(52) Wierzchowski, S. J.; Monson, P. A. *J. Phys. Chem. B* **2007**, *111*, 7274–7282.
(53) Parrish, W. R.; Prausnitz, J. M. *Ind. Eng. Chem. Process Des. Dev.* **1972**, *11*, 26–35.
(54) Barrer, R. M.; Edge, A. V. J. *Proc. R. Soc. London A* **1967**, *300*, 1–24.
(55) Chen, G.-J.; Guo, T.-M. *Chem. Eng. J.* **1998**, *71*, 145–151.
(56) Gil-Villegas, A.; Galindo, A.; Whitehead, P. J.; Mills, S. J.; Jackson, G. *J. Chem. Phys.* **1997**, *106*, 4168–4186.
(57) Galindo, A.; Davies, L. A.; Gil-Villegas, A.; Jackson, G. *Mol. Phys.* **1998**, *93*, 241–252.
(58) Patel, B. H.; Paricaud, P.; Galindo, A.; Maitland, G. C. *Ind. Eng. Chem. Res.* **2004**, *42*, 3809–3823.
(59) Boublík, T. *J. Chem. Phys.* **1970**, *53*, 471–472.
(60) Mansoori, G. A.; Carnahan, N. F.; Starling, K. E.; Leland, T. W. *J. Chem. Phys.* **1971**, *54*, 1523–1525.
(61) Waisman, E.; Lebowitz, J. L. *J. Chem. Phys.* **1970**, *52*, 4307–4309.
(62) Paricaud, P.; Tazi, L.; Borgard, J.-M. *Int. J. Hydrogen Energy* **2010**, *35*, 978–991.
(63) Robinson, R. A.; Stokes, R. H. *Electrolyte Solutions*, 2nd revised ed.; Dover Publications, Inc.: New York, 2002.
(64) Silvester, L. F.; Pitzer, K. S. *J. Solution Chem.* **1978**, *7*, 327–337.
(65) Côté, J.-F.; Perron, G.; Desnoyers, J. E.; Benson, G. C.; Lu, B. C.-Y. *J. Solution Chem.* **1998**, *27*, 685–705.
(66) Valtz, A.; Chapoy, A.; Coquelet, C.; Paricaud, P.; Richon, D. *Fluid Phase Equilib.* **2004**, *226*, 333–344.
(67) Myers, J. A.; Sandler, S. I.; Wood, R. H. *Ind. Eng. Chem. Res.* **2002**, *41*, 3282–3297.
(68) Liu, Z. P.; Wang, W. C.; Li, Y. G. *Fluid Phase Equilib.* **2005**, *227*, 147–156.
(69) Lindenbaum, S.; Boyd, G. E. *J. Phys. Chem.* **1964**, *68*, 911–917.
(70) D'Ans, J.; Surawski, H.; Synowietz, C. Densities of binary aqueous systems and heat capacities of liquid systems. In *Landolt-Börnstein database: numerical data and functional relationships in science and technology. group IV: physical chemistry, mechanical properties*; Hellwege, K.-H., Ed.; Springer: New-York, 1977; Vol. 1b.
(71) Hamer, W. J.; Wu, Y. C. *J. Phys. Chem. Ref. Data* **1972**, *1*, 1047–1099.
(72) Parker, V. B. Thermal properties of aqueous uni-univalent electrolytes; U.S. Dept. of Commerce, National Bureau of Standards, Washington, D.C., 1965.
(73) Kim, D. S.; InfanteFerreira, C. A. *Int. J. Refrig.* **2006**, *29*, 36–46.
(74) Lannung, A. *Z. Phys. Chem.* **1934**, *170*, 134–144.
(75) Patil, K. R.; Tripathi, A. D.; Pathak, G.; Katti, S. S. *J. Chem. Eng. Data* **1990**, *35*, 166–168.
(76) Belveze, L. S.; Brennecke, J. F.; Stadtherr, M. A. *Ind. Eng. Chem. Res.* **2004**, *43*, 815–825.
(77) Amado, A. G.; Blanco, L. H. *Fluid Phase Equilib.* **2005**, *233*, 230–233.
(78) Held, C.; Sadowski, G. *Fluid Phase Equilib.* **2009**, *279*, 141–148.
(79) Mayrath, J. E.; Wood, R. H. *J. Chem. Thermodyn.* **1983**, *15*, 625–632.
(80) Sinha, B.; Sarkar, B. K.; Roy, M. N. *J. Chem. Thermodyn.* **2008**, *40*, 394–400.
(81) Belandria, V.; Mohammadi, A. H.; Richon, D. *J. Chem. Thermodyn.* **2009**, *41*, 1382–1386.
(82) Pickering, S. U. *Ber. Dtsch. Chem. Ges.* **1893**, *26*, 2307–2310.
(83) Pascal, P. *Nouveau Traité de Chimie Minérale, Tome XVI*; Edition Masson et Cie: Paris, 1960.
(84) Steudemann, W. Die thermische Analyse der Systeme desWassers mit den Lithiumhalogeniden; Dissertation, University of Jena, Germany, 1927.
(85) Jones, H. C.; Getman, F. H. *Z. Phys. Chem. Stoechiom. Verwandtschafts.* **1904**, *49*, 385–455.
(86) Lipkowski, J.; Komarov, V. Y.; Rodionova, T. V.; Dyadin, Y. A.; Aladko, L. S. *J. Supramol. Chem.* **2002**, *2*, 435–439.
(87) Darbouret, M. M. Cournil, M.; Herri, J.-M. Rheological study of a hydrate slurry for air conditioning application. *Fifth international conference on gas hydrates*, Trondheim, Norway, 2005.
(88) Sun, Z.-G.; Jiang, C.-M.; Xie, N.-L. *J. Chem. Eng. Data* **2008**, *53*, 2375–2377.
(89) dos Ramos, M. C.; Blas, F. J.; Galindo, A. *Fluid Phase Equilib.* **2007**, *261*, 359–365.
(90) dos Ramos, M. C.; Blas, F. J.; Galindo, A. *J. Phys. Chem. C* **2007**, *111*, 15924–15934.
(91) Houghton, G.; McLean, A. M.; Ritceie, P. D. *Chem. Eng. Sci.* **1957**, *6*, 132–137.
(92) Li, S.; Fan, S.; Wang, J.; Lang, X.; Wang, Y. *J. Chem. Eng. Data* **2010**, *55*, 3212–3215.
(93) Munck, J.; Jørgensen, S. S.; Rasmussen, P. *Chem. Eng. Sci.* **1988**, *43*, 2661–2672.

JP1067457